Fibroblast-specific TGF-β–Smad2/3 signaling underlies cardiac fibrosis

Hadi Khalil,[1] Onur Kanisicak,[1] Vikram Prasad,[1] Robert N. Correll,[1] Xing Fu,[1] Tobias Schips,[1] Ronald J. Vagnozzi,[1] Ruijie Liu,[1,2] Thanh Huynh,[3] Se-Jin Lee,[3] Jason Karch,[1] and Jeffery D. Molkentin[1,4]

[1]Department of Pediatrics, Cincinnati Children's Hospital Medical Center, University of Cincinnati, Cincinnati, Ohio, USA. [2]Department of Biomedical Sciences, Grand Valley State University, Allendale, Michigan, USA. [3]Department of Molecular Biology and Genetics, The Johns Hopkins University School of Medicine, Baltimore, Maryland, USA. [4]Howard Hughes Medical Institute, Cincinnati Children's Hospital Medical Center, Cincinnati, Ohio, USA.

The master cytokine TGF-β mediates tissue fibrosis associated with inflammation and tissue injury. TGF-β induces fibroblast activation and differentiation into myofibroblasts that secrete extracellular matrix proteins. Canonical TGF-β signaling mobilizes Smad2 and Smad3 transcription factors that control fibrosis by promoting gene expression. However, the importance of TGF-β–Smad2/3 signaling in fibroblast-mediated cardiac fibrosis has not been directly evaluated in vivo. Here, we examined pressure overload–induced cardiac fibrosis in fibroblast- and myofibroblast-specific inducible Cre-expressing mouse lines with selective deletion of the TGF-β receptors *Tgfbr1/2*, *Smad2*, or *Smad3*. Fibroblast-specific deletion of *Tgfbr1/2* or *Smad3*, but not *Smad2*, markedly reduced the pressure overload–induced fibrotic response as well as fibrosis mediated by a heart-specific, latency-resistant TGF-β mutant transgene. Interestingly, cardiac fibroblast–specific deletion of *Tgfbr1/2*, but not *Smad2/3*, attenuated the cardiac hypertrophic response to pressure overload stimulation. Mechanistically, loss of *Smad2/3* from tissue-resident fibroblasts attenuated injury-induced cellular expansion within the heart and the expression of fibrosis-mediating genes. Deletion of *Smad2/3* or *Tgfbr1/2* from cardiac fibroblasts similarly inhibited the gene program for fibrosis and extracellular matrix remodeling, although deletion of *Tgfbr1/2* uniquely altered expression of an array of regulatory genes involved in cardiomyocyte homeostasis and disease compensation. These findings implicate TGF-β–Smad2/3 signaling in activated tissue-resident cardiac fibroblasts as principal mediators of the fibrotic response.

Introduction

Heart failure is an increasingly prevalent disease characterized by reduced cardiac output resulting from a progressive loss of cardiomyocytes, ventricular chamber remodeling, and accumulation of interstitial fibrosis (1). Excessive deposition of extracellular matrix (ECM) in heart failure directly restricts normal ventricular function by reducing wall compliance; it also reduces diffusion efficiency, promotes arrhythmia, and possibly limits regenerative efforts of cardiomyocytes (2–4). Progressive cardiac fibrosis in heart failure is predominantly mediated by the tissue-resident cardiac fibroblast, which becomes activated and then differentiated into a cell type referred to as the myofibroblast (5, 6). Activation of fibroblasts within the heart is mediated by inflammatory cytokines, neuroendocrine agonists, stretch of the ventricular wall such as with pressure overload, or following myocardial infarction (MI) injury. In addition to producing and secreting abundant ECM material, myofibroblasts acquire contractile activity through induction of genes such as *Acta2* (α-smooth muscle actin [αSMA]), which allows these cells to physically remodel the ECM or scar after MI (7, 8). While the physiologic function of myofibroblasts is generally beneficial, such as during acute wound healing, sustained activation and continued generation of these cells likely underlie inappropriate developmental remodeling and a wide range of adult fibrotic diseases (9–11). Thus, inhibition of myofibroblast conversion or their activity would be an attractive therapeutic approach in adult fibrotic disease states, including heart failure (12–14).

TGF-β is considered a "master" cytokine/growth factor produced within injured or diseased tissues, where it activates fibroblasts and facilitates ECM production (15, 16). TGF-β binds a heterodimeric receptor in the plasma membrane consisting of the TGF-β type I and type II half-receptors, which together induce phosphorylation of Smad2 and Smad3 transcription factors in mediating canonical signaling. Phosphorylated Smad2 and Smad3 interact with Smad4 in the cytoplasm, where together they translocate to the nucleus to induce gene transcription (17). Activation of the TGF-β type I and II receptors also initiates noncanonical signaling that results in the activation of the MAPK cascade, which culminates in p38, JNK1/2, and ERK1/2 signaling (17).

Global *Smad2*$^{-/-}$ mice are embryonic lethal (18), whereas *Smad3*$^{-/-}$ mice are viable and hence have been examined for alterations in the fibrotic response (8, 19–22). For example, Smad3 underlies the proper induction of TGF-β–responsive genes, such as *Acta2*, *Col1a1*, *Col3a1*, *Fn*, and *Ctgf* (20). Additionally, mice lacking *Smad3* were protected from chemical-induced fibrosis in the kidney (23), fibrosis of the eye (24), and angiotensin II–induced fibrosis of the vasculature (25). With respect to cardiac

Conflict of interest: The authors have declared that no conflict of interest exists.
Submitted: April 25, 2017; **Accepted:** July 26, 2017.
Reference information: *J Clin Invest*. 2017;127(10):3770–3783.
https://doi.org/10.1172/JCI94753.

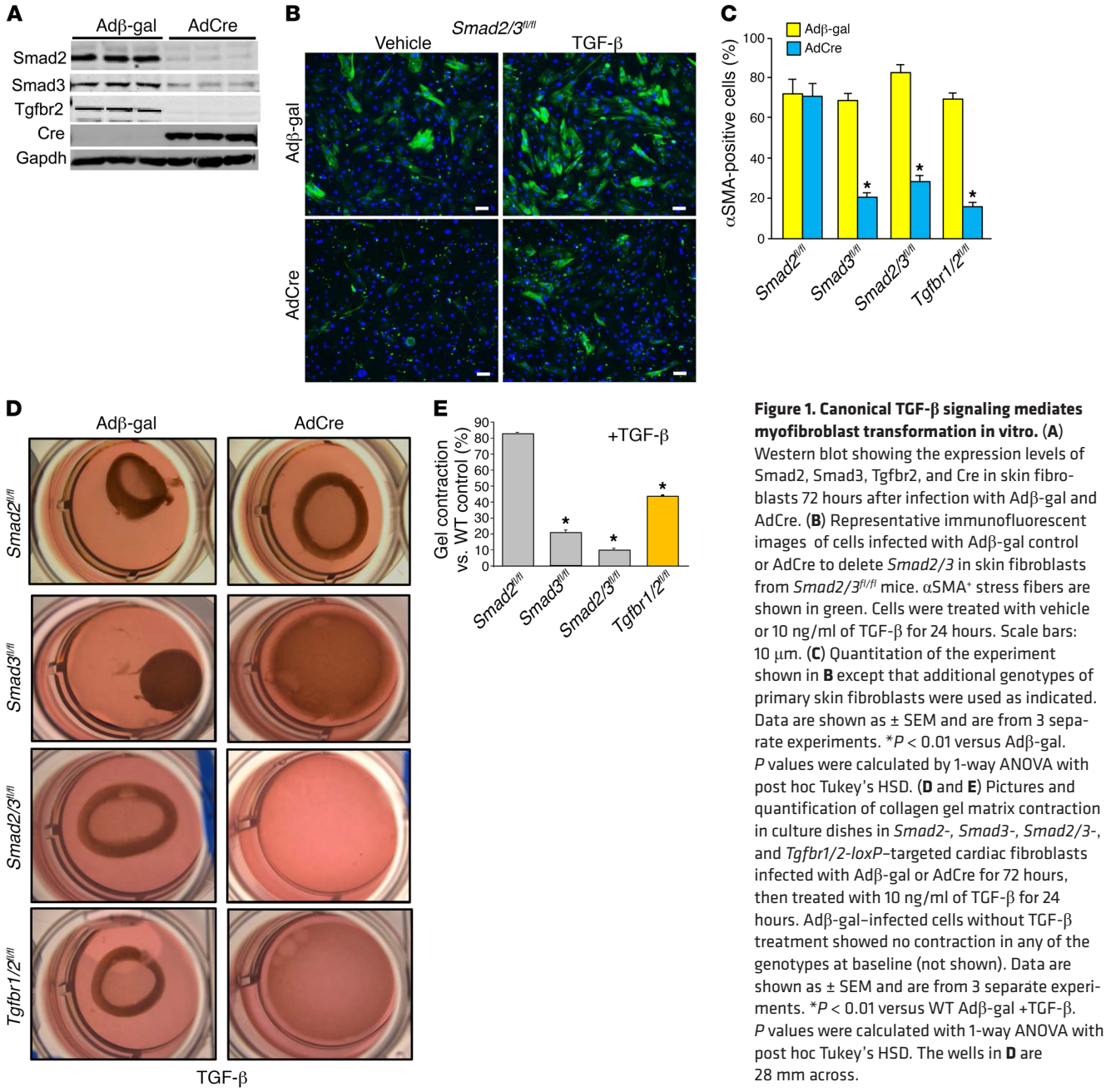

Figure 1. Canonical TGF-β signaling mediates myofibroblast transformation in vitro. (**A**) Western blot showing the expression levels of Smad2, Smad3, Tgfbr2, and Cre in skin fibroblasts 72 hours after infection with Adβ-gal and AdCre. (**B**) Representative immunofluorescent images of cells infected with Adβ-gal control or AdCre to delete *Smad2/3* in skin fibroblasts from *Smad2/3*$^{fl/fl}$ mice. αSMA^{+} stress fibers are shown in green. Cells were treated with vehicle or 10 ng/ml of TGF-β for 24 hours. Scale bars: 10 μm. (**C**) Quantitation of the experiment shown in **B** except that additional genotypes of primary skin fibroblasts were used as indicated. Data are shown as ± SEM and are from 3 separate experiments. *$P < 0.01$ versus Adβ-gal. *P* values were calculated by 1-way ANOVA with post hoc Tukey's HSD. (**D** and **E**) Pictures and quantification of collagen gel matrix contraction in culture dishes in *Smad2-, Smad3-, Smad2/3-*, and *Tgfbr1/2-loxP*–targeted cardiac fibroblasts infected with Adβ-gal or AdCre for 72 hours, then treated with 10 ng/ml of TGF-β for 24 hours. Adβ-gal–infected cells without TGF-β treatment showed no contraction in any of the genotypes at baseline (not shown). Data are shown as ± SEM and are from 3 separate experiments. *$P < 0.01$ versus WT Adβ-gal +TGF-β. *P* values were calculated with 1-way ANOVA with post hoc Tukey's HSD. The wells in **D** are 28 mm across.

studies, global *Smad3*$^{-/-}$ mice showed significantly greater lethality after pressure overload stimulation, although surviving mice showed a 60% reduction in total ventricular fibrosis, with no difference in the degree of cardiac hypertrophy induction compared with controls (19). In a separate study, *Smad3*$^{-/-}$ mice were also shown to have reduced fibrosis in the remote myocardium after MI injury, although scar size was unaffected and total fibroblast content was increased in these injured hearts (26). One limitation of these past studies is a lack of cell-type specificity in attributing how a global deletion of *Smad3* might specifically affect the fibrotic response in the heart. Indeed, cardiomyocyte-specific deletion of *Tgfbr2* from the hearts of mice blocked maladaptive responses to pressure overload stimulation, inhibiting myocyte and interstitial Smad signaling and fibrosis (27). Thus, the cardiomyocyte itself clearly plays a role in TGF-β–Smad2/3 signaling and fibrosis in the diseased heart. Here we utilized 2 recently developed fibroblast-specific inducible Cre-expressing mouse lines to selectively delete *Tgfbr1* and *Tgfbr2* versus *Smad2* and *Smad3* to examine how canonical signaling at the level of the fibroblast underlies fibrosis and disease responsiveness of the heart.

Results

Canonical TGF-β effectors Smad2/3 promote myofibroblast differentiation. To examine the possible differential role between Smad2 and Smad3 as mediators of TGF-β receptor signaling, we generated primary skin fibroblasts from mice with loxP site (fl) targeted alleles for *Smad2*, *Smad3*, and *Smad2/3* and compared them with fibroblasts conditionally targeted within the *Tgfbr1 and Tgfbr2* loci.

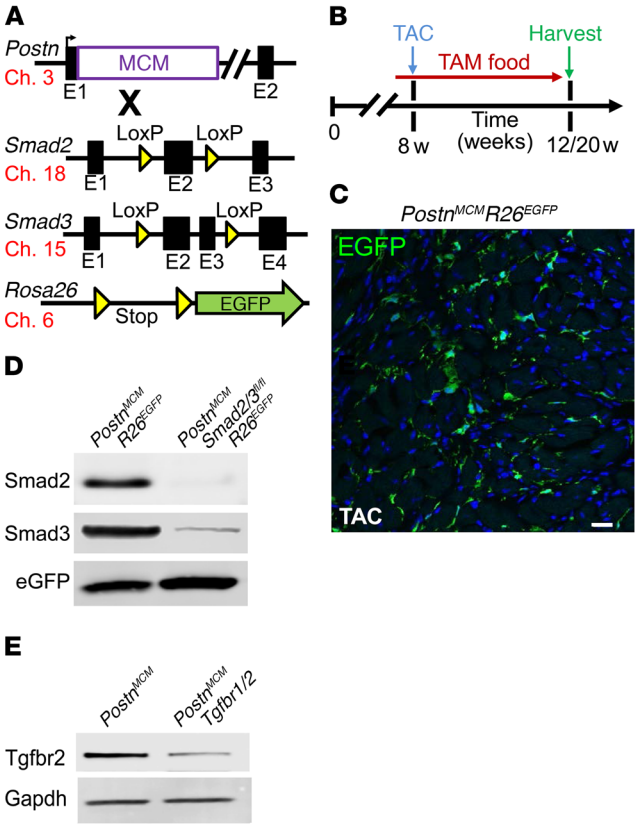

Figure 2. Generation of fibroblast-specific canonical TGF-β–deleted mice. (**A**) Schematic representation of different mouse lines used, including the *Postn* genetic locus containing a tamoxifen-regulated MCM cDNA cassette inserted into exon 1 (E1), which was crossed with *Smad2*- and/or *Smad3-loxP*–containing gene-targeted lines, along with the *Rosa26* reporter allele(*R26*^{EGFP}). The mouse chromosome associated with each allele is shown. (**B**) Experimental scheme whereby mice were subjected to TAC injury or sham procedure for 4 and 12 weeks. Mice were fed tamoxifen diet 48 hours before surgery and then maintained on tamoxifen until harvesting. (**C**) Representative histological section showing EGFP-labeled interstitial cells in hearts of *Postn*$^{MCM/+}$ *R26*$^{EGFP/+}$ mice after 4 weeks of TAC injury (n = 4). Scale bar: 10 μm. (**D**) Western blot analysis for Smad2, Smad3, and EGFP from 500,000 cells isolated from hearts of the 2 genotypes of mice shown. (**E**) Western blot for Tgfbr2 in total heart mesenchymal cells lacking myocytes, CD31, and CD45 cells and conditionally targeted for *Tgfbr1/2-loxP* with *Postn*^{MCM} in cardiac-activated fibroblasts after TAC stimulation.

These primary skin fibroblasts were infected with a Cre-expressing adenovirus (AdCre) and compared with a control β-gal–expressing (Adβ-gal–expressing) adenovirus (Figure 1A). Western blotting of protein extracts from these primary fibroblasts 72 hours after recombinant adenoviral infection showed efficient deletion of Smad2 and Smad3 protein from *Smad2/3*$^{fl/fl}$ double-homozygous cells with AdCre and efficient deletion of *Tgfbr2* in *Tgfbr1/2*$^{fl/fl}$ homozygous cells (Figure 1A). Control and AdCre-infected *Smad2*$^{fl/fl}$, *Smad3*$^{fl/fl}$, and *Smad2/3*$^{fl/fl}$ primary fibroblasts were stimulated with TGF-β and assayed for differentiation into myofibroblasts, as marked by αSMA expression. The data show that 70%–80% of the Adβ-gal–infected *Smad2*$^{fl/fl}$, *Smad3*$^{fl/fl}$, and *Smad2/3*$^{fl/fl}$ or *Tgfbr1/2*$^{fl/fl}$ fibroblasts became αSMA positive with TGF-β stimulation, while AdCre infection blocked this induction with deletion of *Smad3*, *Smad2/3*, or *Tgfbr1/2*, but not *Smad2* (Figure 1, B and C).

Targeted primary cardiac fibroblasts were also seeded into Matrigel for contraction assays as a more specific assessment of TGF-β–induced myofibroblast formation with contractile activity (Figure 1D). Here, we observed robust gel contraction in WT fibroblasts (not shown) and all the genotypes of primary cardiac fibroblasts tested that were infected with Adβ-gal (Figure 1, D and E). AdCre-infected *Smad2*$^{fl/fl}$ fibroblasts also showed full gel contraction comparable to that of WT fibroblasts with TGF-β stimulation (Figure 1, D and E). However, AdCre infection of *Smad3*$^{fl/fl}$, *Smad2/3*$^{fl/fl}$, and *Tgfbr1/2*$^{fl/fl}$ fibroblasts showed inhibition in TGF-β–induced gel contraction (Figure 1, D and E). These results indicate that the 2 central TGF-β receptors and Smad3 are critical mediators of myofibroblast differentiation and function in vitro with TGF-β stimulation, but that Smad2 was not necessary for this response.

Activated fibroblast-specific Smad2-, Smad3-, and Smad2/3-deleted mice. Previous genetic-based studies designed to inhibit TGF-β signaling in heart disease models have lacked selectivity for the fibroblast (19, 26–28). Hence, here we used mice in which the *Postn* genetic locus was targeted with a tamoxifen-inducible MerCreMer (MCM) cDNA (29), and these mice were crossed with *Smad2*$^{fl/fl}$, *Smad3*$^{fl/fl}$, *Smad2/3*$^{fl/fl}$, and *Tgfbr1/2*$^{fl/fl}$ targeted mice (Figure 2A). We also introduced a single *Rosa26-loxP-Stop-loxP-EGFP* (*R26*^{EGFP}) reporter allele to allow irreversible tracking of all activated fibroblasts, as previously described (29). Importantly, periostin expression is specifically induced in essentially all activated fibroblasts (myofibroblasts) of the heart with injury (30–32). Young adult mice were subjected to cardiac pressure overload stimulation by transverse aortic constriction (TAC) surgery over 4 to 12 weeks in the presence of tamoxifen food so that the MCM protein could mediate recombination in activated fibroblasts (Figure 2B). Indeed, immunohistochemistry in *Postn*$^{MCM/+}$ *R26*$^{EGFP/+}$ mice over 4 weeks of TAC in the presence of tamoxifen showed EGFP expression in activated fibroblasts throughout the heart (Figure 2C), as previously characterized in detail (29). In an identical experiment in mice that also contained the *Smad2/3*$^{fl/fl}$ alleles, EGFP-labeled cells were subjected to FACS and pooled for Western blotting to assess the degree to which Smad2 and Smad3 proteins were deleted from activated cardiac fibroblasts after 4 weeks of TAC. The results showed almost complete absence of these 2 proteins compared with similarly sorted control fibroblasts that were not targeted for the *Smad2/3* alleles (Figure 2D). A similar strategy in *Tgfbr1/2*$^{fl/fl}$ *Postn*$^{MCM/+}$ mice was performed in which cardiomyocyte-free total mesenchymal cells were negatively sorted to remove CD31- and CD45-expressing cells and protein extracts generated, which showed an approximate 80% deletion of Tgfbr2 protein (Figure 2E). These results indicate that the *Postn*^{MCM} allele effectively deletes loxP-targeted genes from activated fibroblasts from the heart.

Role of Smad2, Smad3, and Tgfbr1/2 in fibroblast-dependent cardiac fibrosis with pressure overload. TAC was performed in young adult mice for 4 or 12 weeks to assess pressure overload–induced cardiac fibrosis in which *Smad2*, *Smad3*, *Smad2/3*, or *Tgfbr1/2* was specifically deleted from activated fibroblasts (Figure 2B). Levels of fibrosis and collagen deposition in each genotype were assessed by Masson's trichrome staining of cardiac histological sections (Figure 3, A and B, and Supplemental Figure 1A, and Supplemental Figure 2;

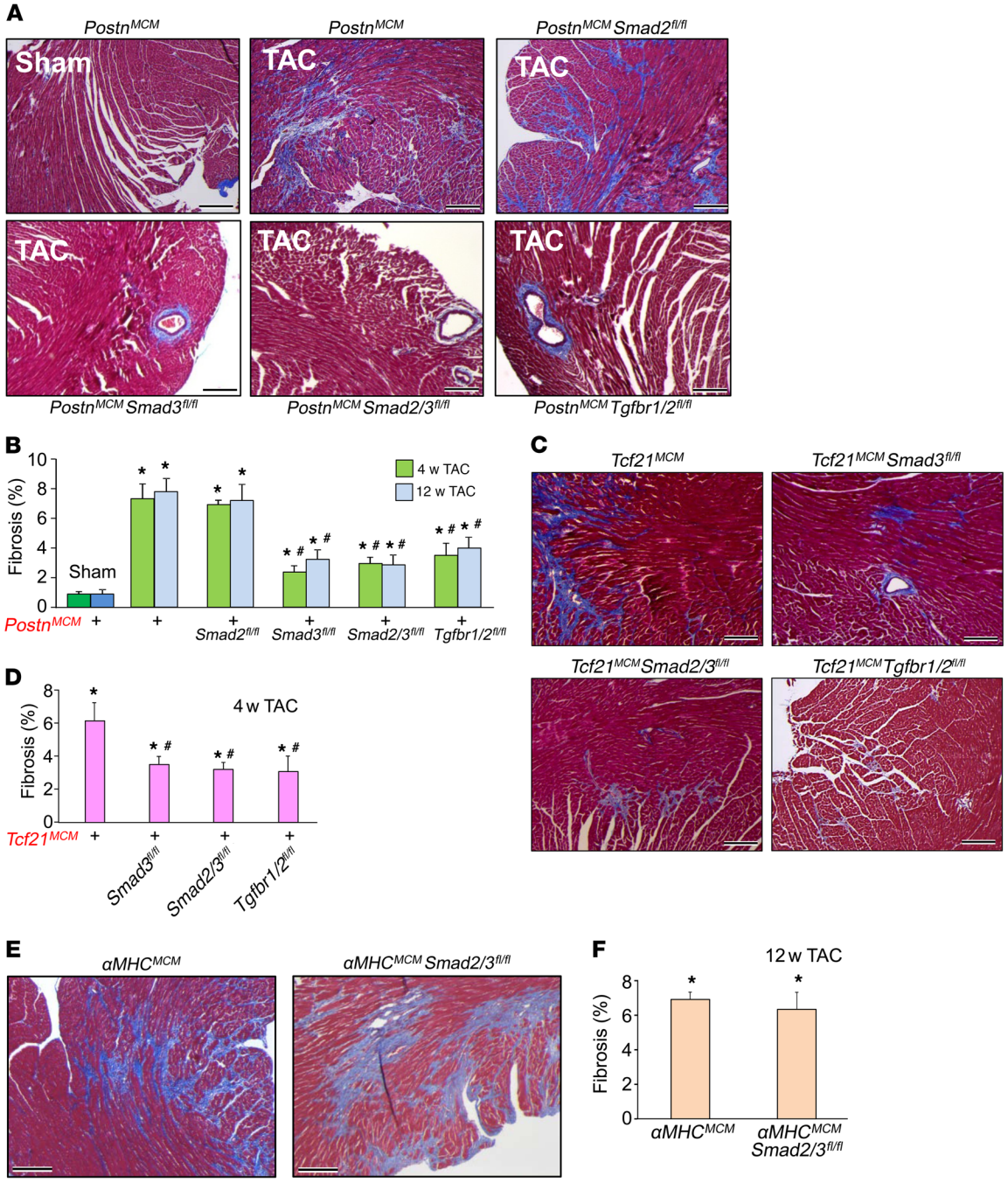

Figure 3. Fibroblast-specific deletion of canonical TGF-β signaling reduces myocardial fibrosis in mice. (**A** and **B**) Masson's trichrome–stained histological pictures and quantitation of the area of fibrosis (blue) in hearts from the indicated genotypes of mice with Postn$^{MCM/+}$ after 12 weeks of TAC injury and tamoxifen treatment. Average fibrotic area ± SEM. n = 8–10 mice in each group. *P < 0.05 versus sham operated; #P < 0.05 versus Postn$^{MCM/+}$ TAC at 4 or 12 weeks. P values were calculated by 1-way ANOVA with post hoc Tukey's HSD. (**C** and **D**) Masson's trichrome–stained histological photographs and quantification of the area of fibrosis in hearts from the indicated mice crossed with Tcf21$^{MCM/+}$ after 4 weeks of TAC injury and tamoxifen treatment. Average fibrotic area ± SEM. n = 6–9 mice in each group, *P < 0.05 versus sham operated; #P < 0.05 versus Tcf21$^{MCM/+}$ TAC at 4 weeks. P values were calculated by 1-way ANOVA with post hoc Tukey's HSD. (**E** and **F**) Masson's trichrome–stained histological photographs and quantification of the area of fibrosis in αMHC$^{MCM/+}$ and cardiomyocyte-specific deletion of Smad2/3 from hearts after 12 weeks of TAC injury. Mice were injected 5 times with 100 μl of 0.5 mg/ml of tamoxifen 15 days before injury. Average fibrotic area ± SEM. n = 7–9 mice in each group. *P < 0.05 versus sham operated. P values were calculated using 1-way ANOVA with post hoc Tukey's HSD. Scale bars: 150 μm.

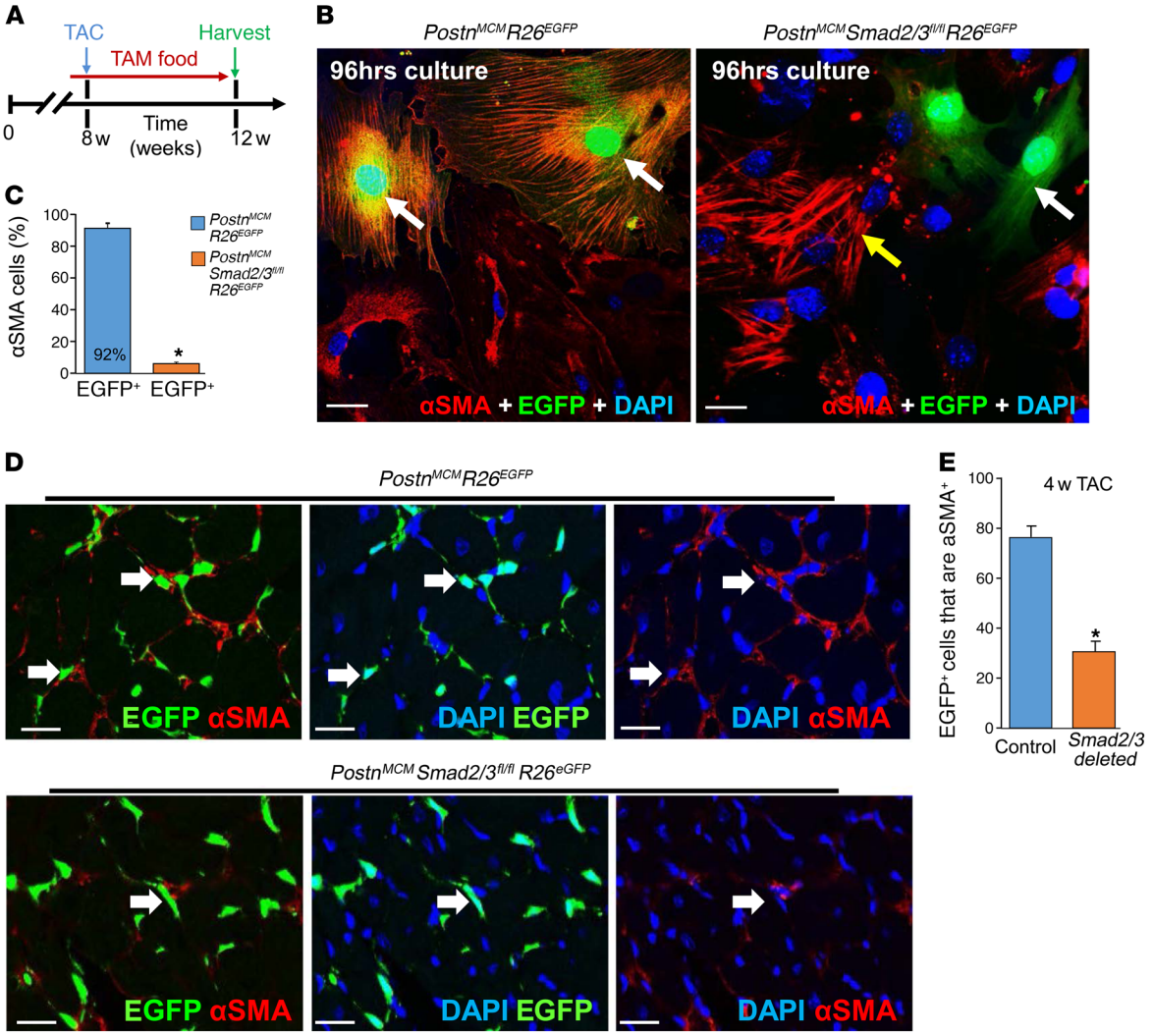

Figure 4. Fibroblast-specific *Smad2/3* deletion alters myofibroblast activity in vivo. (**A**) Experimental scheme whereby mice were subjected to TAC for 4 weeks. Mice were fed tamoxifen-laden chow 48 hours before surgery and then until harvesting. (**B** and **C**) Representative immunostaining images and quantitation for EGFP⁺ cellular expression (green) and costaining for αSMA (red) and DAPI (blue) in isolated cardiac interstitial cells from the indicated genotypes of mice that were cultured for 96 hours in low serum medium. The white arrows indicate EGFP⁺ cells and the yellow arrow shows EGFP⁻ cells that are αSMA⁺ (n = 4). *P < 0.05 versus *Postn*$^{MCM/+}$ *R26*$^{EGFP/+}$ cells. P values were calculated with Student's t test. Scale bars: 10 μm. (**D** and **E**) Representative immunohistochemistry cryosections and quantitation of EGFP-labeled (green) interstitial cells along with αSMA (red) staining from hearts of the indicated genotypes of mice after 4 weeks of TAC. The white arrows show EGFP⁺ cells that are also αSMA⁺ in each of the 2 genotypes of mice, although in the *Smad2/3*-deleted hearts, most of the EGFP⁺ fibroblasts are deficient in αSMA expression (n = 4 mice in each group). *P < 0.05 versus *Postn*^{MCM} *R26*^{EGFP} hearts. P values were calculated with Student's t test. Scale bars: 10 μm. Additional images of immunohistochemistry as shown in **D** are shown in Supplemental Figure 5.

supplemental material available online with this article; https://doi.org/10.1172/JCI94753DS1). The data show that deletion of *Smad3*, *Smad2/3*, or *Tgfbr1/2*, but not *Smad2*, significantly attenuated the cardiac fibrotic response to pressure overload following 4 and 12 weeks of TAC stimulation (Figure 3, A and B). Because Smad2 and Smad3 are transcription factors that have been implicated in directly mediating expression of myofibroblast genes (17, 20, 33–38), we assessed mRNA levels of endogenous *Postn*, *Col1a1*, and *Col3a1* from primary cardiac fibroblasts treated with TGF-β in culture. The data show a generalized and significant reduction in expression of these 3 activated fibroblast marker genes in both *Smad3*- and *Smad2/3*-deleted fibroblasts, but not with deletion of *Smad2* (Supplemental Figure 3, A–C). These data indicate that deleting canonical TGF-β signaling constituents from newly activated fibroblasts significantly reduces the cardiac fibrotic response, although *Smad2* appeared to be fully compensated by the remaining *Smad3* gene.

In parallel, echocardiography at 4 and 12 weeks after TAC was employed to determine whether loss of *Smad2/3* or *Tgfbr1/2* signaling from activated fibroblasts affected heart function and/or the hypertrophic response. Twelve weeks of TAC stimulation resulted in a significant reduction in ventricular fractional shortening in control mice (controls consisted of *Postn*$^{MCM/+}$ alone or *Smad2/3*$^{fl/fl}$ alone) versus sham-operated mice (Supplemental Figure 4A). Deletion of *Smad2*, *Smad3*, or *Smad2/3* from activated fibroblasts resulted in the same significant reduction in ventricular fractional shortening as seen in the controls after TAC, although deletion of

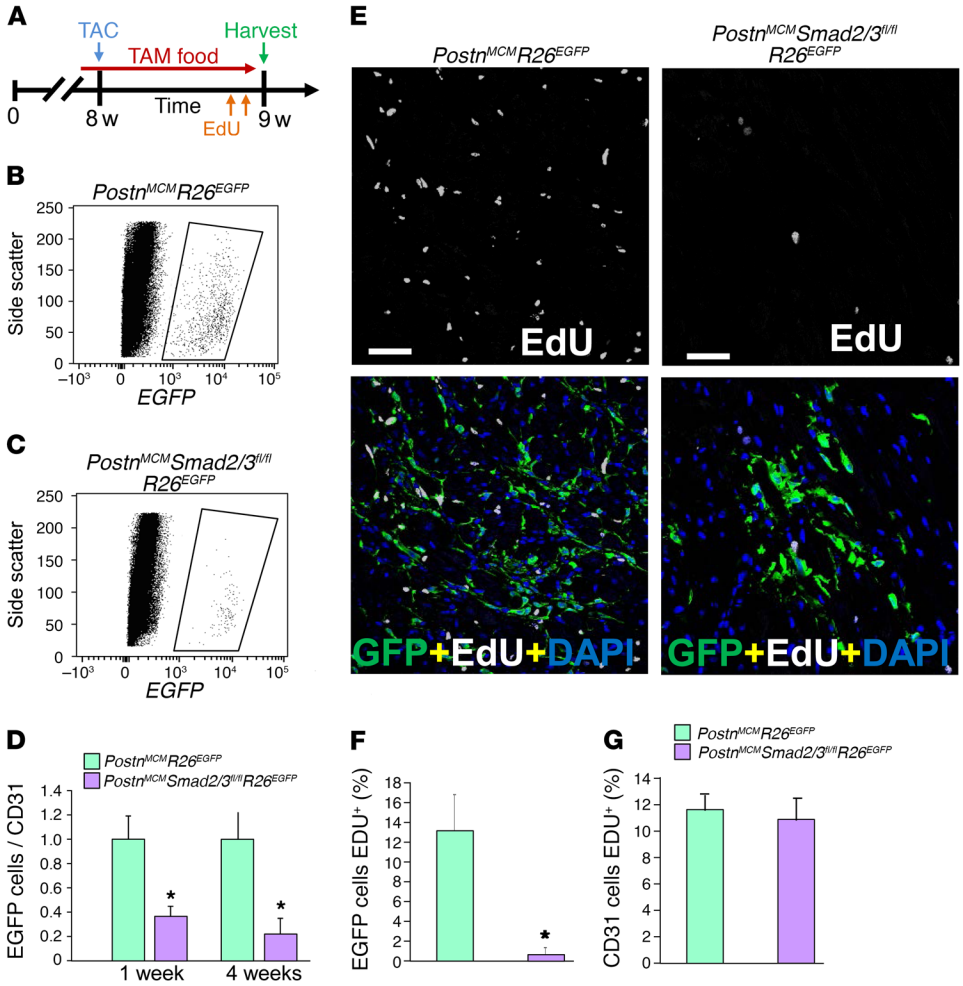

Figure 5. Fibroblast-specific *Smad2/3* deletion reduces the number of activated myofibroblasts in vivo. (**A**) Experimental schematic whereby mice were subjected to TAC injury for 7 days. Mice were fed tamoxifen-laden chow 48 hours before surgery and then until harvesting. EdU was injected into mice 24 hours and 4 hours before harvest. (**B** and **C**) Representative flow cytometry plots of isolated EGFP$^+$ interstitial cells (rightward scatter) from hearts of the indicated genotypes of mice. (**D**) The ratio of total GFP$^+$ activated fibroblasts normalized to CD31$^+$ cells from the heart taken from the indicated genotypes of mice after 1 or 4 weeks of TAC. Error bars represent SEM. $n = 3$ mice in each group. $^*P < 0.05$ versus *Postn*$^{MCM/+}$ *R26*$^{EGFP/+}$. *P* values were calculated with Student's *t* test. (**E** and **F**) Representative immunohistological images and quantitation of the percentage of EGFP$^+$ interstitial cells costained for EdU (white) according to the schematic in **A**. DAPI was used to show nuclei (blue). $n = 3$ mice in each group. $^*P < 0.05$ versus *Postn*$^{MCM/+}$ *R26*$^{EGFP/+}$. *P* values were calculated with Student's *t* test. Scale bars: 50 μm. (**G**) Quantitation of CD31-positive cells that were also EdU positive in heart histological sections from mice subjected to TAC of the indicated genotypes. Representative images of the CD31-positive cells with EdU staining along with GFP-positive fibroblasts from histological heart sections are shown in Supplemental Figure 6.

Tgfbr1/2 significantly protected from this profile of reduced ventricular performance (Supplemental Figure 4A). Similarly, *Smad2*, *Smad3*, and *Smad2/3* fibroblast–targeted mice showed a similar degree of cardiac hypertrophy following 12 weeks of TAC as controls, yet deletion of *Tgfbr1/2* with *Postn*$^{MCM/+}$ resulted in significantly less cardiac hypertrophy (Supplemental Figure 4B, see Discussion). In support of these data, histological analysis of cardiomyocyte cell surface areas in hearts of these same mice showed significantly less hypertrophy with *Tgfbr1/2* deletion after 4 weeks of TAC compared with controls or *Smad2/3* deletion after TAC, while *Smad2/3* heart–specific deleted mice showed the same level of hypertrophy as WT mice (control sham = 281 ± 10 μm^2, control TAC = 483 ± 12 μm^2, *Smad2/3* deleted = 494 ± 12 μm^2, *Tgfbr1/2* deleted = 309 ± 8 μm^2; $P < 0.05$ versus control TAC, $n = 4$ mice in each group). We also performed a more advanced echocardiographic procedure with strain analysis 4 weeks after TAC. The data showed a trend toward reduced longitudinal left ventricular wall strain in *Smad2/3* double-deleted mice compared with control or *Tgfbr1/2*-KO mice after TAC (Supplemental Figure 4C). Interestingly, diastolic function measured indirectly by pulse-wave and tissue Doppler echocardiography indicated a lower *E*/*e*′ ratio (where *E* indicates E wave and *e*′ indicates peak tissue velocity) in *Tgfbr1/2* double-deleted mice after TAC compared with control or *Smad2/3* double-deleted mice, suggestive of preserved diastolic function (Supplemental Figure 4D).

One possible limitation with the *Postn*^{MCM} allele is that it requires fibroblast activation before the loxP-targeted gene under investigation would be deleted. Hence, *Smad2/3* would likely become partially induced before deletion occurs with the *Postn*$^{MCM/+}$ allele. To deal with this hypothetical situation, we employed an independent tamoxifen-inducible Cre-expressing gene-targeted mouse line in which the transcription factor 21 (*Tcf21*) allele is targeted with the MCM cDNA (*Tcf21*^{MCM}). We and others have shown that the *Tcf21*$^{MCM/+}$ allele is expressed in essentially all tissue-resident fibroblasts in the uninjured heart, but no other cell types, and that these cells beget the activated fibroblasts (29, 39). Here, we used 4 weeks of TAC with tamoxifen treatment in *Tcf21*$^{MCM/+}$ mice crossed with *Smad3*$^{fl/fl}$, *Smad2/3*$^{fl/fl}$, and *Tgfbr1/2*$^{fl/fl}$ mice. We again observed the same significant reduction in cardiac fibrosis as with the *Postn*$^{MCM/+}$ allele crossed with these same loxP-targeted genes (Figure 3, C and D, and Supplemental Figure 1B). Hence, deletion of *Smad2/3* with the *Tcf21*^{MCM} allele from cardiac fibroblasts before they become activated is similarly effective in attenuating the disease-dependent fibrotic response, as observed with the slightly later induced *Postn*^{MCM} allele.

Deletion of *Tgfbr1* or *Tgfbr2* from cardiomyocytes of the heart was shown to protect from cardiac fibrosis and functional decompensation with remodeling following pressure overload (27). Here, we deleted *Smad2/3* from the adult heart using the α-myosin heavy chain (αMHC) MCM-containing transgene (40) to determine

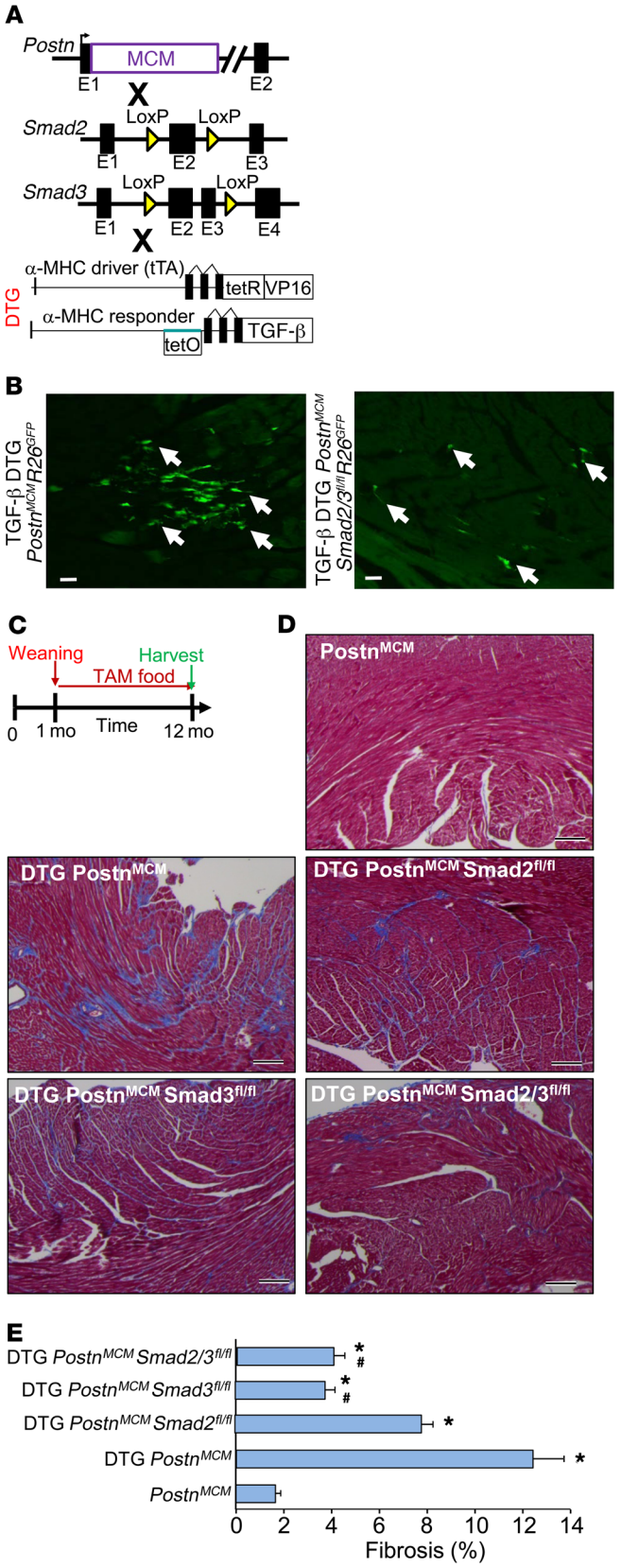

Figure 6. Fibroblast-specific deletion of *Smad2/3* reduces TGF-β–induced myocardial fibrosis. (**A**) Schematic representation of *Postn*^{MCM} mice crossed to *Smad2*- and/or *Smad3-loxP* mice in conjunction with an inducible heart-specific latency-escaping TGF-β mutant cDNA driven by a cardiomyocyte-specific DTG system. (**B**) Representative histological heart sections with GFP$^+$ interstitial cells (white arrows) showing that the TGF-β DTG effectively mediated Cre-dependent induction of *Postn*$^{MCM/+}$activity, facilitating R26^{EGFP} recombination and expression, while deletion of *Smad2/3* reduced total EGFP$^+$ cells. Hearts were harvested 4 weeks after tamoxifen administration. n = 4 mice harvested. Scale bars: 10 μm. (**C**) Experimental schematic whereby data shown in **D** and **E** were from mice fed tamoxifen through 12 months of age. (**D** and **E**) Pictures of Masson's trichrome–stained cardiac histological sections and quantitation of the area of fibrosis (blue staining) in the indicated genotypes of mice in the presence of the TGF-β mutant transgenic system (DTG) for 12 months. Data are shown as average fibrotic area ± SEM. n = 6–8 in each group. $^*P < 0.05$ versus *Postn*$^{MCM/+}$; $^{\#}P < 0.05$ versus DTG *Postn*$^{MCM/+}$. P values were calculated by 1-way ANOVA with post hoc Tukey's HSD. Scale bars: 150 μm.

whether canonical Smad2/3 signaling within cardiomyocytes might similarly affect the cardiac fibrotic response with pressure overload. However, unlike deletion of *Smad2/3* from cardiac fibroblasts, as presented above, deletion of *Smad2/3* specifically from cardiomyocytes of mice with 12 weeks of pressure overload showed no ability to inhibit the fibrotic response compared with *αMHC*^{MCM} controls (Figure 3, E and F, and Supplemental Figure 1C). Thus, the ability of Smad2/3 transcriptional activity to support disease-mediated cardiac fibrosis appears to be largely specific to the cardiac fibroblast.

Deletion of Smad2/3 compromises myofibroblasts in vivo. Deletion of *Smad2/3* from resting or activated fibroblasts in the hearts of mice subjected to TAC substantially reduced the fibrotic response, although the cellular basis for this reduction in fibrosis was unknown. Here, we examined the fate of activated fibroblasts/myofibroblasts in the heart following *Smad2/3* deletion. *Postn*$^{MCM/+}$ *R26*$^{EGFP/+}$ mice were used as a control versus the same genotype of mice that also contained the *Smad2/3*$^{fl/fl}$ alleles, and young adults were subjected to 4 weeks of TAC with tamoxifen chow administration (Figure 4A). We first removed hearts from these mice and isolated total interstitial cells and cultured them as a mixed population (Figure 4B). Interestingly, we observed that approximately 90% of EGFP$^+$ control cells replete with the *Smad2/3* alleles became αSMA positive in culture yet nearly all the EGFP$^+$ cells in the *Smad2/3* targeted interstitial cell pool were devoid of αSMA expression and lacked the characteristic stress fibers of myofibroblasts (Figure 4, B and C). We also performed direct analysis of EGFP$^+$ versus αSMA-expressing cells in the heart from the same 2 groups of mice after 4 weeks of TAC (Figure 4D). The data show that 78% of EGFP$^+$ *Postn*-traced activated fibroblasts in the heart are also αSMA expressing when *Smad2/3* are present, while only 30% overlap was observed when *Smad2/3* are deleted from activated cardiac fibroblasts (Figure 4, D and E, and Supplemental Figure 5). Indeed, most of the EGFP$^+$ fibroblasts in the hearts of *Postn*$^{MCM/+}$ *Smad2/3*$^{fl/fl}$ mice after 4 weeks of TAC lacked αSMA expression (Figure 4D).

To analyze fibroblast proliferation rates, mice of the genotype *Postn*$^{MCM/+}$ *Smad2/3*$^{fl/fl}$ *R26*$^{EGFP/+}$ were compared with controls of the genotype *Postn*$^{MCM/+}$ *R26*$^{EGFP/+}$ and subjected to 1 or 4 weeks of TAC stimulation with tamoxifen administration to trace fibroblasts (Figure 5A). Importantly, at the 1-week time point, 5-ethynyl-2′-deoxyuridine (EdU) was given in the last 24 hours before sacrifice so that proliferation rates could be directly assessed (Figure 5A). Hearts were then collected from these 2 groups of mice and digested and total EGFP$^+$ cells counted and normalized to CD31$^+$ (Supplemental Figure 6) or Erg1$^+$ (data not shown) endothelial cells as an approxi-

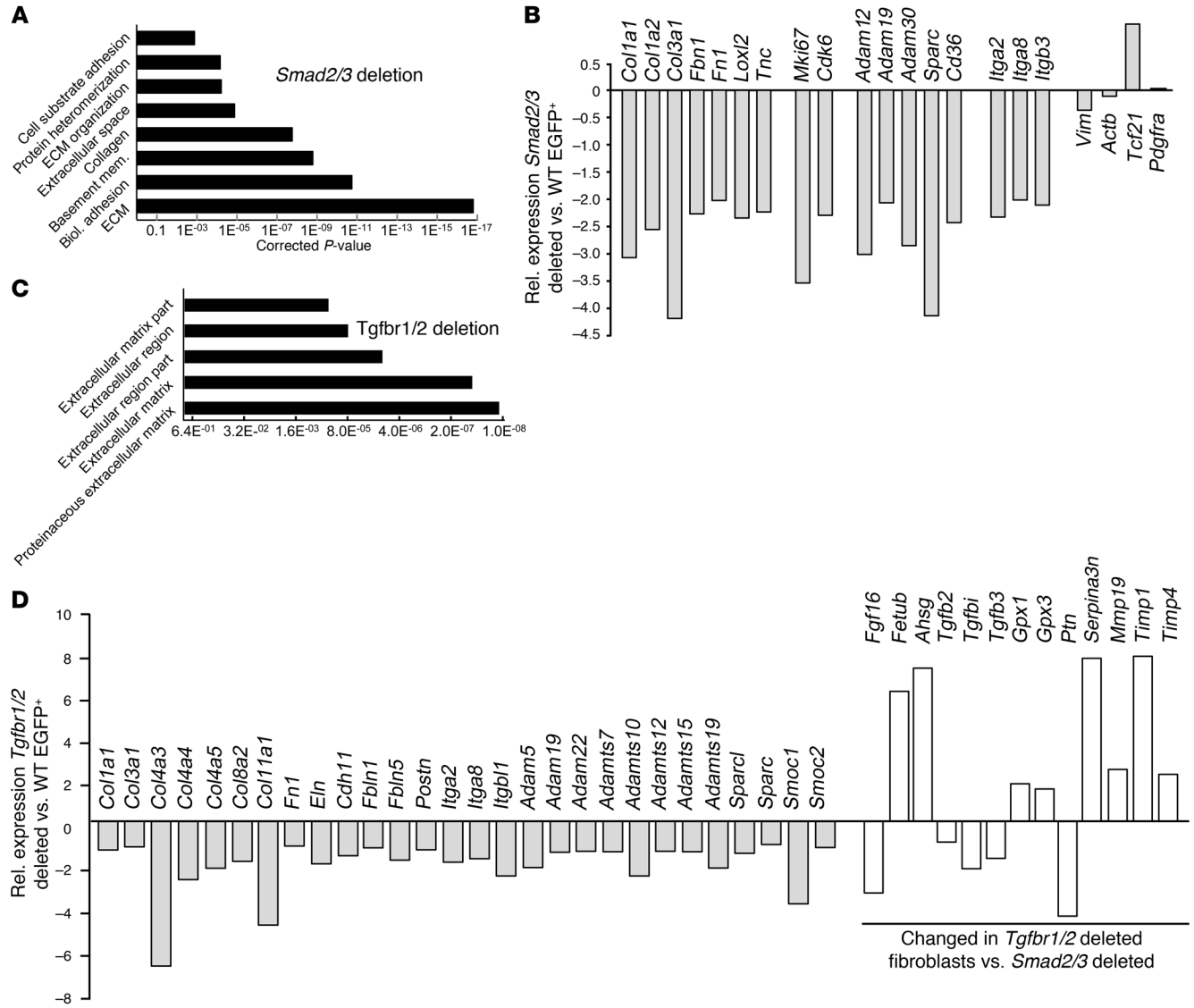

Figure 7. *Smad2/3* deletion in activated fibroblasts reduces fibroblast and ECM-related gene expression. (**A**) Gene expression cluster analysis showed a profile of altered ECM and fibrosis-related gene expression in EGFP$^+$ fibroblasts obtained from hearts of *Smad2/3*-activated fibroblast-deleted mice versus control WT hearts, isolated 4 weeks after TAC injury. (**B**) Quantification of selected mRNAs in *Smad2/3*-deleted EGFP$^+$-activated fibroblasts from hearts of *Smad2/3 Postn*$^{MCM/+}$ *R26*$^{EGFP/+}$ allele–containing mice. (**C**) Gene expression cluster analysis shows a profile of altered ECM- and fibrosis-related gene expression in EGFP$^+$ fibroblasts obtained from hearts of *Tgfbr1/2* fibroblast–deleted mice versus control WT hearts, isolated 4 weeks after TAC injury. (**D**) Quantification of selected mRNAs in *Tgfbr1/2*-deleted EGFP$^+$ fibroblasts from hearts of *Tgfbr1/2 Tcf21*$^{MCM/+}$ *R26*$^{EGFP/+}$ allele–containing mice. The white bars in **D** represent genes altered in expression compared with those with deletion of *Smad2/3*.

mation of activated fibroblast expansion and endothelial cell proliferation with EdU administration. While endothelial cells do expand with pressure overload stimulation, it is generally less than 30% (41, 42), and this effect was the same between our 2 experimental groups with or without *Smad2/3* in activated cardiac fibroblasts (Figure 5G and Supplemental Figure 6). The data show a dramatic reduction in total activated EGFP$^+$ fibroblasts in the hearts of *Smad2/3*-deleted mice after 4 weeks of TAC compared with control mice replete with *Smad2/3* in their activated fibroblasts (Figure 5, B–D). Even with 1 week of TAC, there was a significant reduction in EGFP$^+$ activated fibroblasts when *Smad2/3* were deleted from these cells (Figure 5D).

Histological sections were also directly quantified for EGFP$^+$ fibroblasts or immunostained for endothelial cells that were positive or negative for EdU incorporation (Figure 5, E–G, and Supplemental Figure 6). The data show that over 24 hours of EdU exposure, 13% of EGFP$^+$ activated fibroblasts incorporated EdU, suggesting the cells were actively proliferating, while approximately 1% of the *Smad2/3*-deleted EGFP$^+$ activated fibroblasts incorporated EdU (Figure 5, E and F). As a control, there was equivalent proliferation of endogenous endothelial cells between the 2 groups with TAC stimulation to the heart (Figure 5G). Also as an important control, loss of *Smad2/3* or *Tgfbr1/2* from primary skin fibroblasts did not differentially affect their sensitivity to cell death through apoptosis with staurosporine in culture compared with WT (Supplemental Figure 7). Thus, loss of *Smad2/3* from disease-activated fibroblasts in the heart compromises their dif-

ferentiation and proliferation, but not cell death, suggesting a cellular mechanism for the observed reduction in fibrosis in mice in which *Smad2/3* are deleted from cardiac fibroblasts.

Smad2/3 deletion from fibroblasts compromises TGF-β–induced fibrosis in the heart. To confirm and extend our observations to this point, a cardiac-specific, latency-escaping mutant TGF-β–expressing (TGF-β1^{Cys223,225Ser}) transgene was used, which we previously showed induces interstitial cardiac fibrosis (43). Double transgenic (DTG) mice with this bigenic inducible system were crossed with *Smad2*$^{fl/fl}$, *Smad3*$^{fl/fl}$, or *Smad2/3*$^{fl/fl}$ mice (Figure 6A, no doxycycline was given so that the transgene was always active). The *R26*^{EGFP} allele was also present and tamoxifen was administered beginning at 4 weeks of age so that fibroblasts could be visualized and directly assessed in vivo. The data show that EGFP$^+$ cells were observed in the heart at 2 months of age, suggesting that the TGF-β transgene induced *Postn*^{MCM} activity in activated fibroblasts (Figure 6B), while control mice without the TGF-β DTG system showed essentially no EGFP$^+$ cells in the ventricles at 2 months (data not shown). We observed substantially fewer EGFP$^+$ traced fibroblasts in the hearts of TGF-β DTG mice in the absence of *Smad2/3* (Figure 6B).

We next performed a chronic fibrosis study in which TGF-β DTG mice were put on tamoxifen (without doxycycline, for full induction) at 4 weeks of age and followed for 1 year before the hearts were harvested (Figure 6C). Masson's trichrome analysis showed that TGF-β DTG mice with the *Postn*$^{MCM/+}$ allele had fibrosis in their hearts by 12 months of age compared with hearts from WT or *Postn*$^{MCM/+}$ mice lacking the TGF-β transgene (Figure 6, D and E, and Supplemental Figure 1D). However, deletion of *Smad3* alone or *Smad2/3* from activated fibroblasts of these same TGF-β DTG *Postn*$^{MCM/+}$ mice showed a significant reduction in cardiac fibrosis compared with the TGF-β DTG *Postn*$^{MCM/+}$ control mice (Figure 6, D and E, and Supplemental Figure 1D). As observed with TAC stimulation, deletion of *Smad2* was not effective in reducing the cardiac fibrotic response, as these mice showed significant fibrosis that was not statistically different from that in TGF-β DTG *Postn*$^{MCM/+}$ control mice (Figure 6E). Hence, Smad3 appears to be the dominant effector of TGF-β–induced cardiac fibrosis in the mouse heart, while Smad2 appears to be fully compensated by the presence of Smad3.

Gene expression alterations in Smad2/3- versus Tgfbr1/2-deficient fibroblasts. To gain further insight into the molecular basis for Smad2/3-dependent regulation of fibroblast activity and fibrosis, global RNA-sequencing (RNA-Seq) profiling was performed. EGFP$^+$ cells were obtained by FACS from hearts of *Postn*$^{MCM/+}$ *R26*$^{EGFP/+}$ versus *Postn*$^{MCM/+}$ *Smad2/3*$^{fl/fl}$ *R26*$^{EGFP/+}$ mice 4 weeks after TAC injury. Bioinformatics analysis of the data showed a gene expression signature in which many of the top categories of gene pathways were related to the activity or function of myo/fibroblasts or the ECM (Figure 7A). For example, the expression of direct ECM mRNAs *Col1a1*, *Col1a2*, *Col3a1*, *Fn1*, *Fbn1*, and *Tnc* in EGFP$^+$ fibroblasts showed significantly reduced levels in the absence of *Smad2/3*. Also downregulated were the ECM-modifying genes *Loxl2*, *Adam12*, *Adam30*, and *Sparc* along with the cell-adhesion genes *Itga2*, *Itga8*, and *Itgb3* (Figure 7B). Key proliferation genes such as *Mki67* and *Cdk6* were significantly downregulated in *Smad2/3*-deleted fibroblasts as well (Figure 7B), which is consistent with the known profile of compromised proliferation of these cells observed in vivo after injury (Figure 5). No significant changes were observed between the 2 genotypes of fibroblasts analyzed in the relative expression of the global fibroblast identity markers *Tcf21*, *Pdgfra*, and *Vimr* or in a housekeeping gene such as *Actb* (Figure 7B).

EGFP$^+$ cells were also obtained from hearts of *Tcf21*$^{MCM/+}$ *R26*$^{EGFP/+}$ versus *Tcf21*$^{MCM/+}$ *Tgfbr1/2*$^{fl/fl}$ *R26*$^{EGFP/+}$ mice 4 weeks after TAC injury. Bioinformatics analysis of these data showed a gene expression signature similar to that found with *Smad2/3* deletion in that most of the top categories of gene pathways were related to the activity or function of fibroblasts and the ECM (Figure 7C). Hence, the overwhelming effect associated with deletion of the 2 TGF-β receptors from cardiac fibroblasts with pressure overload stimulation is an alteration in fibrosis and ECM-associated gene expression (Figure 7, C and D). As with *Smad2/3* deletion, we observed downregulation of a large array of fibrosis, adhesion, and ECM genes such as *Col1a1*, *Col3a1*, *Col4a3*, *Col11a1*, *Fn1*, *Fbn1*, *Sparc*, *Itga2*, *Itga8*, *Eln*, *Postn*, and *Adams* (Figure 7D). However, loss of *Tgfbr1/2* from cardiac fibroblasts also substantially altered expression of genes not observed with deletion of *Smad2/3*, and many of these had interesting regulatory implications, such as a decrease in *Tgfb2*, *Tgfbi*, and *Tgfb3* (Figure 7D). Also of interest, *Fgf16* and *Ptn* are known protective factors in the heart (44–46) that were each substantially downregulated with loss of *Tgfbr1/2* (Figure 7D). Other genes implicated in cardiac homeostasis, such as *Ahsg*, *Fetub*, *Gpx1*, *Gpx3*, *Serpina3n*, *Ptn*, *Timp1*, and *Timp4*, were also uniquely changed in the absence of *Tgfbr1/2*, but not with *Smad2/3* deletion (Figure 7D). Some of these genes could contribute to the differential cardiac compensatory and hypertrophy effects shown in Supplemental Figure 4.

Discussion

Global TGF-β activity is upregulated in diseased hearts, where one of its primary actions is directed at the resident fibroblasts to alter the fibrotic response and ventricular remodeling (47, 48). However, all previous studies that manipulated TGF-β signaling in the heart either used mice with global *Smad3* deletion, which results in loss of SMAD3 protein in all cells (19, 26), mice with cardiac-specific deletion of *Tgfbr1* or *Tgfbr2*, or mice treated with systemically acting drugs or blocking antibodies that do not distinguish cell type of action (27, 28, 49). In this study, we uniquely interrogated the cardiac fibroblast as a putative mediator of heart disease in vivo. Our results indicate that the tissue-resident cardiac fibroblast is primarily responsible for mounting a fibrotic response with pressure overload stimulation. These results indicate that *Smad2/3* are critical in the induction and maintenance of activated fibroblast activity and productive fibrosis in the heart in response to pressure overload or the TGF-β ligand itself. In comparison, deletion of *Smad2/3* specifically from cardiomyocytes was ineffective in altering the pressure overload cardiac fibrotic response.

Another interesting observation was that deletion of *Smad2* from activated fibroblasts did not diminish their activation profile, ability to induce αSMA, ability to contract a collagen gel, or ability to mediate a fibrotic response in vivo. In contrast, deletion of *Smad3* from activated fibroblasts compromised the differentiated function and activity of these cells in culture and in vivo. While *Smad2*$^{-/-}$ mice have not been extensively studied given their embryonic lethal phenotype, our results with the conditional loxP-targeting approach suggest that this transcription factor is not central to the fibrotic

response from the standpoint of the activated fibroblast. However, our results in *Smad3-loxP*–targeted mice in which this gene was only deleted from activated fibroblasts were consistent with data from global *Smad3*$^{-/-}$ mice in which the cardiac fibrotic response was reduced following pressure overload or MI injury (19, 20, 26).

With respect to Smad3 being more important than Smad2 in mediating fibroblast activation and fibrosis in vivo, one simple explanation could be that Smad3 is more highly expressed in cardiac fibroblasts, although this does not appear to be the case (Figure 2D). Indeed, others have also reported that Smad3 appears to function dominantly over Smad2 in other systems. For example, Smad3 dominates over Smad2 in regulating TGF-β–dependent chondrogenic differentiation (50). Moreover, Smad3, but not Smad2, is part of a transcriptional regulatory complex with histone deacetylase-1 (HDAC1) in binding to the PPARγ promoter in mouse cardiac fibroblasts (51). In hepatic stellate cells (fibroblasts), knockdown of *Smad3* reduced TGF-β–induced type 1a collagen expression while knockdown of *Smad2* increased its expression and Smad2 overexpression reduced type 1a collagen expression (52). Finally, transcriptional profiling in Hep3B cells showed that knockdown of *Smad2* versus *Smad3* resulted in 190 genes being differentially controlled, and again, Smad3 was dominant over Smad2 in how TGF-β affected these cells (53).

Loss of *Smad2/3* rendered newly activated fibroblasts in the heart less proliferative and compromised in their differentiated function and ability to express fibrosis-mediating genes. A wealth of past literature suggests that Smad2/3 directly bind to the promoters of fibrosis and myofibroblast-dependent genes to modulate their expression characteristics (17, 20, 33–38, 52, 53). Here, we observed that loss of *Smad2/3* from activated cardiac fibroblasts rendered them unable to induce or even maintain normal baseline expression of fibrosis-dependent signature genes, while loss of *Smad2* was of little effect. Such a defect in fibroblast gene expression would have obvious functional implications on newly activated fibroblasts in vivo, hence explaining the observed phenotype in mice with *Smad2/3* deletion mediated by the *Postn*^{MCM} allele in response to cardiac pressure overload. Fibroblast proliferation was also compromised in pressure-overloaded hearts when *Smad2/3* were deleted from activated fibroblasts, again partially explaining why the fibrotic response in these hearts was attenuated.

While deletion of *Smad2/3* from fibroblasts reduced cardiac fibrosis during 12 weeks of pressure overload stimulation, it did not alter the ultimate decompensation of these hearts as assessed by echocardiography (fractional shortening) or the hypertrophy of these hearts by gravimetric analysis. In dramatic contrast, deletion of *Tgfbr1/2* genes from activated fibroblasts of pressure-overloaded hearts similarly reduced expression of fibrosis-mediating genes, but it uniquely benefitted the hearts of these mice such that they did not show a reduction in left ventricular fractional shortening, and the degree of cardiac hypertrophy was reduced compared with that of controls. On the surface, this observation might simply reflect the fact that Tgfbr1/2 signaling is upstream of both canonical (Smad2/3) and noncanonical (MAPK) TGF-β signaling. Canonical signaling through Smad2/3 could be more dedicated to direct regulation of fibrosis-mediating genes, while noncanonical signaling such as through p38α MAPK, which we recently showed is also critical for fibrosis (54), might have additional complexity in augmenting expression of genes that directly control other regulatory pathways in the heart that affect hypertrophy or compensation with injury. Indeed, global mRNA profiling of fibroblasts deleted for *Tgfbr1/2* showed altered expression for an array of important cardiac regulatory genes that was not observed with Smad2/3 deletion (Figure 7D). Any one of these genes, or more likely, the entire profile of uniquely changed genes could easily underlie the observed phenotypic differences in compensation and pressure overload–induced hypertrophy observed between *Tgfbr1/2* and *Smad2/3* fibroblast–deleted mice.

The observations presented here suggest a bifurcation point in attempting future therapeutic strategies aimed at TGF-β for affecting cardiac fibrosis with longstanding chronic disease states. The ability to selectively block canonical signaling through Smad2/3 should reduce fibrosis itself without altering other growth-dependent effects of TGF-β. Alternatively, blocking all upstream noncanonical TGF-β signaling would similarly have an effect on cardiac fibrosis, but could also be additionally protective to the heart by reducing other maladaptive signaling effects. Indeed, deletion of *Mapk14* from activated fibroblasts of the heart reduced fibrosis with MI injury or neuroendocrine agonists (54). Thus, targeting one aspect of TGF-β signaling as an antifibrotic approach might circumvent the known ineffectualness associated with drugs or antibodies that globally block TGF-β signaling (55). Moreover, designing delivery methods to specifically target the activated fibroblast might also provide selectivity that limits side effects associated with total systemic TGF-β inhibition (55).

Methods

Mice. Mice containing a knockin of a MCM cDNA into either the *Postn* or *Tcf21* genomic loci were previously described (29, 39). αMHC-MCM transgenic mice (40) and TGF-β tTA DTG transgenic mice (56) were previously described. *Tgfbr1/2-loxP*–targeted mice were previously described (27). *Rosa26* reporter mice (*R26*^{EGFP}) were previously described (57) and were purchased from the Jackson Laboratory (catalog 012429). LoxP-targeted *Smad2/3* mice were recently described as well (58). PCR genotyping used the primers *Smad3* forward 5′-GTTTACTGGACTGAGGTTGGCTGTGGC-3′ and reverse 5′-GTACAGATTGGCCACTCCGGTCACTG-3′, which generated a 390-bp product recognizing loxP-targeted exons 2/3 and 287-bp WT fragments. *Smad2* genotyping primers 5′-ATAATGGGTCCCAGTAACACCGGAC-3′ and 5′-CTCAAACCTTACCAAGCCAAAGCAG-3′ generated a 400-bp product recognizing the loxP-containing site in exon 2 and a 360-bp WT fragment. αMHC-MerCreMer mice received i.p. injections with pharmaceutical grade tamoxifen (20 mg/kg body weight) dissolved in 95% peanut oil/ 5% ethanol for 5 consecutive days 15 days before the surgical procedure. Postn-MerCreMer mice received continuous tamoxifen-citrate chow feeding (40 mg/kg body weight, Envigo - TD.130860) 48hrs before a procedure and then until the experiment was terminated. Tcf21-MerCreMer mice received 15 days of tamoxifen food before a procedure that continued until harvest. All strains of mice were in the C57BL/6 genetic background.

Animal procedures. Eight- to ten-week-old male mice of the relevant genotypes were subjected to pressure overload by TAC surgery. A silk ligature was tied around the aorta together with 26-gauge blunted needle between the origins of the right innominate and left common carotid artery, after which the needle was removed to generate a defined con-

striction. A sham surgical procedure was identical, but without ligature placement. Echocardiography was performed to assess ventricular geometry and function at 4 and 12 weeks after TAC. Echocardiography was performed in mice under 2% isoflurane inhalation anesthesia (until effect), and measurements were performed using a Hewlett Packard 5500 instrument with a 15-MHz microprobe and recorded on M-mode in triplicate for each mouse and averaged. Doppler echocardiography was performed on mice subjected to TAC to measure pressure gradients across the aortic constriction to verify the effectiveness of the TAC procedure.

For analysis of longitudinal strain and diastolic function by echocardiography, a Vevo 2100 instrument with 18–38 MHz transducer (VisualSonics) was used as previously described (59). Longitudinal B-mode loops of 300 frames each were analyzed using VevoLAB speckle-based tracking (VisualSonics) to determine average longitudinal strain across the left ventricle. For indirect measurement of diastolic function, pulse-wave Doppler echocardiography was performed across the mitral valve leaflets in an apical long-axis view to determine peak flow velocity (E wave). Tissue Doppler was performed in a short-axis view at the level of the papillary muscles to determine peak tissue velocity (*e′*) of the LV posterior wall. The ratio of these measures (*E/e′*) was used as an indicator of diastolic function (60).

Histology and immunostaining. Isolated hearts were fixed for 4 hours in freshly diluted 4% paraformaldehyde at 4°C. Part of the tissue was rinsed with PBS and cryoprotected in 30% sucrose/PBS overnight before embedding in OCT (Tissue-Tek). Another part was washed with 70% ethanol and subjected to paraffin embedding. Afterwards, 10-μm cryosections were collected and then blocked for 30 minutes at room temperature in a blocking solution (PBS with 5% goat serum, 2% bovine serum albumin, 0.1%Triton X-100). Sections were then incubated with primary antibody against αSMA (Sigma-Aldrich, A2547) diluted in blocking solution overnight at 4°C at 1:200 dilution. Sections were washed 3 times for 5 minutes each in PBS and incubated with a 1:500 dilution of Alexa Fluor 568–conjugated (Life Technologies, A11031) goat anti-mouse antibody for 2 hours at room temperature at 1:500 dilutions. After washing 3 times for 5 minutes each, sections were stained with DAPI at a concentration of 0.1 μg/ml in PBS for 5 minutes at room temperature and mounted on slides using aqueous mounting medium (H-1400, Vector Laboratories). Cryosections were occasionally used to visualize native EGFP fluorescence from the different genotypes with the *Rosa26*-containing loxP-dependent reporter allele. Images were acquired with an inverted Nikon A1R confocal microscope using NIS Elements AR 4.13 software. Masson's trichrome staining was performed with a kit (Sigma-Aldrich, HT15-1KT) per the manufacturer's instructions. Trichrome images were captured with a Leica M165FC stereo microscope with fluorescence using a Leica DFC310 FX camera and the Leica Application Suite. Picrosirius red staining was performed with a kit (Abcam ab150681) per the manufacturer's instructions. Picrosirius red and polarized light images were captured at ×200 magnification by an Olympus BX51 microscope equipped with a single chip color CCD camera (DP70) and DP controller software (Olympus America Inc.). Images were analyzed with Adobe Photoshop CS5.

Proliferation measurement. Six days after TAC, mice were treated with EdU (61135-33-9, Santa Cruz Biotechnology Inc.) dissolved in PBS with 2 separate i.p. injections over 24 hours (5 μg/g of body weight/day). Four hours after the second EdU injection, hearts were fixed in 4% paraformaldehyde and frozen for immunohistochemical analysis. Cryosections were costained with anti-EGFP antibody (ab13970, Abcam) along with anti-CD31 (Miltenyi Biotec, 130-097-418) or anti-Erg1 (Abcam, Ab92513), then sections were incubated with a 1:500 dilution of goat anti-chicken Alexa Fluor 488 and goat anti-rabbit Alexa Fluor 568 secondary antibodies (A-11039 and A-11036, Life Technologies), followed by EdU staining using a Click-iT EdU Alexa Fluor 647 Imaging Kit (C10643, Life Technologies). Pictures were taken with a Nikon A1 confocal microscope. Three random pictures of the left ventricle free wall were taken from 3 sections at different levels for quantitative analysis. For myofibroblast proliferation, only EGFP/EdU/DAPI-positive cells were counted. For endothelial cell proliferation, CD31/EdU/DAPI cells were counted.

Western blot. Western blotting was performed as described previously (61). Briefly, after electrophoresis and transfer to PVDF membranes, the membranes were incubated with antibodies against Smad2 (1:1000 Cell Signaling, 5339S), Smad3 (1:500 Abcam, ab28379), Cre (1:1000 Novagen, 69050), EGFP (1:1000 Santa Cruz Biotechnology Inc., SC-9996), Tgfbr2 (1:1000 Abcam, 186838), and Gapdh (1:10000 Fitzgerald, 10R-G109a). PVDF membranes were then incubated with the appropriate Alexa Fluor–conjugated secondary antibodies (Thermo Fisher Scientific, A-21057, A11367) and visualized using an Odyssey CLx imaging system (LI-COR Biosciences, 9140). Full and uncropped Western blot gel images for all the figures are shown in Supplemental Figure 8.

Fibroblast cultures and treatments. Adult skin and heart fibroblasts were cultured in DMEM (Fisher Scientific, SH30022FS) supplemented with 10% FBS and nonessential amino acids. Depending on the experiment, cells were then infected with Adβ-gal or AdCre recombinase–expressing adenovirus and maintained for 72 hours. Myofibroblast differentiation was analyzed by counting cells positive for αSMA stress fibers by immunocytochemistry 24 hours after differentiation induction with recombinant porcine TGF-β (10 ng/ml, 101-B1-001, R&D Systems). The same procedure was used for collagen gel contraction assays, although 72 hours after infection, 50,000 cells were seeded into collagen gel matrices and then were induced to differentiate with 10 ng/ml of recombinant TGF-β in DMEM media supplemented with 2% FBS. Gels were released, and the area of contraction was measured after 24 additional hours.

Adult heart interstitial cell isolation. Adult cardiomyocytes were isolated from freshly beating hearts cannulated for retrograde perfusion with a modified Tyrode solution (120 mM NaCl, 14.7 mM KCl, 0.6 mM KH_2PO_4, 0.6 mM Na_2HPO_4, 1.2 mM $MgSO_4$, 10 mM HEPES, 4.6 mM $NaHCO_3$, 30 mM taurine, 5.5 mM glucose, and 10 mM butanedionemonoxime [BDM], pH7.4) supplemented with Liberase TH (Roche, 05401151001). After perfusion, hearts were disassociated into cardiomyocytes and noncardiomyocyte fractions and aggregated by 2 serial centrifugations at 10 *g* for 5 minutes at 4°C. The noncardiomyocyte cell fraction was collected after a final centrifugation at 500 *g* for 10 minutes at 4°C. Endothelial ($CD31^+$) and myeloid ($CD45^+$) cell fractions were sorted with a Magnetic Cell Isolation and Cell Separation Kit (Miltenyi Biotec) with antibodies against CD31 (Miltenyi Biotec, 130-097-418) and CD45 (Miltenyi Biotec, 130-052-301) using the manufacturer's recommended conditions.

Isolation of adult cardiac or skin fibroblasts. Cardiac ventricles or patches of skin were excised from mice, rinsed with cold sterile HBSS, and treated as described previously (29). Briefly, tissues were thoroughly minced with sterile fine scissors and digested in 10 ml DMEM containing Worthington collagenase type 2 (LS004177) (0.2%) at 37°C for 90 minutes. During this incubation, the digesting

tissue was triturated for a minute with a sterile serological pipette every 15 minutes. The supernatant cell suspension containing liberated fibroblasts was then collected into a tube containing cold DMEM. The undigested fraction was reconstituted with fresh digestion media, and the same digestion procedure was repeated until almost the entire tissue was dissociated into single cells. Cell debris was eliminated by 2 serial centrifugations at 10 *g* for 5 minutes at 4°C, and the cell fraction was collected after a final centrifugation at 500 *g* for 10 minutes at 4°C. Pellets were washed once with ice-cold HBSS and resuspended in 2% FCS in HBSS and incubated on ice for FACS analysis using a BD Aria Instrument. A fraction of this preparation was cultured in DMEM media supplemented with 10% FBS on 0.1% gelatin-coated plates for further in vitro analysis.

Flow cytometry and cell sorting. Flow cytometry analysis was performed on isolated cardiac interstitial cells using BD FACSCanto II running FACSDiva software with the following configuration: 405 nm laser for Alexa Fluor 405, 633 nm for APC, and 488 nm for EGFP. Voltages were determined using single-stain and fluorescence minus one controls. Analysis was performed using FlowJo vX software (FLOWJO LLC). Cells were stained with APC-conjugated antibodies against CD31 (eBioscience 17-0311-82) at a 1:200 dilution in 2% FCS in HBSS incubated for 30 minutes on ice. Cells were then washed 3 times with ice-cold HBSS and incubated for another 30 minutes on ice with 2% FCS and 0.1% Triton-X 100 in HBSS containing secondary antibody conjugated to Alexa Fluor 647. At the end of the incubation time, cells were washed 3 times and analyzed. For analysis of lineage-traced genotypes, we utilized the endogenous EGFP fluorescence expressed by the recombined reporter allele described above under *Mice*. The count of $EGFP^+$ cells was normalized to the number of $CD31^+$ cells to assure similar digestion of samples and to eliminate differences in total counts due to sample preparation variability. Quantification of total isolated $CD31^+$ endothelial cells was also performed to assess proliferation in the different genotypes versus fibroblasts.

RNA-Seq and bioinformatic analysis. Total RNA was amplified using the Ovation RNA-Seq System v2 (NuGEN, 7102-32) according to the manufacturer's protocol. The libraries were prepared with the Nextera XT DNA Sample Preparation Kit (Illumina Technologies, FC-131-1002). One nanogram of cDNA was suspended in Tagment DNA Buffer, and tagmentation (fragmentation and tagging with the adaptors) was performed with the Nextera enzyme (Amplicon Tagment Mix, FC-131-1096), incubating at 55°C for 10 minutes. Libraries were prepared by PCR with the Nextera PCR Master Mix, and 2 Nextera Indexes (N7XX, and N5XX) according to the following program: 1 cycle of 72°C for 3 minutes; 1 cycle of 98°C for 30 seconds,; 12 cycles of 95°C for 10 seconds, 55°C for 30 seconds, and 72°C for 1 minute; and 1 cycle of 72°C for 5 minutes. The purified cDNA was captured on an Illumina flow cell for cluster generation. Libraries were sequenced on the Illumina HiSeq2500 following the manufacturer's protocol. Bioinformatic analysis of data was carried out using Strand NGS software (ver. 2.6; Build: mouse mm10 [UCSC] using Ensembl transcript annotations) to identify differentially expressed genes. Gene clustering analysis of pathway gene expression groupings was done with Strand NGS software. The RNA-Seq data were deposited in the NCBI's Gene Expression Omnibus (GEO GSE101772).

Reverse-transcriptase PCR. RNA was isolated from fibroblasts using QIAshredder homogenization and the RNAeasy Kit according to the manufacturer's instructions (QIAGEN, catalog 74104). Total RNA was reverse transcribed using random oligo-dT primers and a Verso cDNA Synthesis Kit (Thermo Fisher, AB1453) according to the manufacturer's instructions. Real-time PCR was performed using SsoAdvanced SYBR Green (Bio-Rad, 6090), and Rpl7 expression was used for normalization. The following primer sets were used to identify transcripts: collagen 1a1, 5′-AATGGCACGGCTGTGTGCGA and 5′-AACGGGTCCCCTTGGGCCTT; collagen 3a1, 5′-TCCCCTGGAATCTGTGAATC and 5′-TGAGTCGAATTGGGGAGAAT; periostin, 5′-ACGGAGCTCAGGGCTGAAGATG and 5′- GTTTGGGCCCTGATCCCGAC.

Cell death analysis. At 90% confluence, primary skin fibroblasts were treated with 200 nM staurosporine for 36 hours or vehicle (DMSO). Cell death was determined by the Muse Count & Viability Assay (Millipore, MCH100102) as previously described (62). Briefly, the medium was collected with the trypsin-liberated cells, which were centrifuged and washed twice with PBS and then incubated with the Muse Count & Viability reagent. The cells were then quantified on a Muse cell analyzer (Millipore) at 5,000 counts per sample.

Statistics. One-way ANOVA with post hoc Tukey's honest significant difference (HSD) or Student's *t* test was used to determine statistical significance, depending on the type of data analyzed and number of comparisons. *P* values of less than 0.05 were considered statistically significant. Averaged data are presented with SEM to indicate variability.

Study approval. Mice were observed daily and cages changed weekly by certified veterinary technicians at Cincinnati Children's Hospital Medical Center. Mice were also closely assessed for their well-being, monitored by adequate physical activity and food intake on a daily basis. Housing conditions and husbandry conformed to AAALAC standards as well as the standard guidelines from the NIH Office of Laboratory Animal Welfare (http://grants.nih.gov/grants/olaw/animal_use.htm). The institution also retains ongoing certification by AAALAC. All animal experimentation and this specific study were approved by the Office of Research Compliance and Regulatory Affairs and by the Cincinnati Children's Hospital Institutional Animal Care and Use Committee (protocol number IACUC 2016-0069, expires 11-2019). No human subjects were used.

Author contributions

HK, OK, TS, RNC, RL, RJV, JK, and XF conducted all experimentation. TS performed Matrigel contractions assay. RNC and RL performed TAC surgery. XF conducted EdU experiments. VP conducted bioinformatics analysis. RJV performed echocardiography. JK performed cell death assays. HK and OK designed and conducted experiments and acquired and analyzed data. TH and SJL designed and generated the *Smad2/3-loxP*–targeted mice. JDM and HK conceived the study, directed the study, and wrote the manuscript.

Acknowledgments

This work was supported by grants from the NIH and by the Howard Hughes Medical Institute to JDM. HK was supported by the Swiss National Science Foundation (project P2LAP3_148429 and P300P3_158486). SJL was supported by a grant from the NIH (R01AR060636).

Address correspondence to: Jeffery D. Molkentin, Cincinnati Children's Hospital Medical Center, Howard Hughes Medical Institute, Heart Institute, 240 Albert Sabin Way, MLC 7020, Cincinnati, Ohio 45229 USA. Email: jeff.molkentin@cchmc.org.

1. Benjamin EJ, et al. Heart disease and stroke statistics-2017 update: a report from the American Heart Association. *Circulation*. 2017;135(10):e146–e603.
2. Bowers SL, Banerjee I, Baudino TA. The extracellular matrix: at the center of it all. *J Mol Cell Cardiol*. 2010;48(3):474–482.
3. Fan D, Takawale A, Lee J, Kassiri Z. Cardiac fibroblasts, fibrosis and extracellular matrix remodeling in heart disease. *Fibrogenesis Tissue Repair*. 2012;5(1):15.
4. Xie M, Burchfield JS, Hill JA. Pathological ventricular remodeling: therapies: part 2 of 2. *Circulation*. 2013;128(9):1021–1030.
5. Souders CA, Bowers SL, Baudino TA. Cardiac fibroblast: the renaissance cell. *Circ Res*. 2009;105(12):1164–1176.
6. Takeda N, et al. Cardiac fibroblasts are essential for the adaptive response of the murine heart to pressure overload. *J Clin Invest*. 2010;120(1):254–265.
7. Hinz B. The myofibroblast: paradigm for a mechanically active cell. *J Biomech*. 2010;43(1):146–155.
8. Wynn TA. Cellular and molecular mechanisms of fibrosis. *J Pathol*. 2008;214(2):199–210.
9. Henderson NC, Forbes SJ. Hepatic fibrogenesis: from within and outwith. *Toxicology*. 2008;254(3):130–135.
10. Scotton CJ, Chambers RC. Molecular targets in pulmonary fibrosis: the myofibroblast in focus. *Chest*. 2007;132(4):1311–1321.
11. Gourdie RG, Dimmeler S, Kohl P. Novel therapeutic strategies targeting fibroblasts and fibrosis in heart disease. *Nat Rev Drug Discov*. 2016;15(9):620–638.
12. Asano Y. Future treatments in systemic sclerosis. *J Dermatol*. 2010;37(1):54–70.
13. Bonafoux D, Lee WC. Strategies for TGF-beta modulation: a review of recent patents. *Expert Opin Ther Pat*. 2009;19(12):1759–1769.
14. Declèves AE, Sharma K. New pharmacological treatments for improving renal outcomes in diabetes. *Nat Rev Nephrol*. 2010;6(6):371–380.
15. Dobaczewski M, Chen W, Frangogiannis NG. Transforming growth factor (TGF)-beta signaling in cardiac remodeling. *J Mol Cell Cardiol*. 2011;51(4):600–606.
16. Leask A. Potential therapeutic targets for cardiac fibrosis: TGFbeta, angiotensin, endothelin, CCN2, and PDGF, partners in fibroblast activation. *Circ Res*. 2010;106(11):1675–1680.
17. Derynck R, Zhang YE. Smad-dependent and Smad-independent pathways in TGF-beta family signalling. *Nature*. 2003;425(6958):577–584.
18. Nomura M, Li E. Smad2 role in mesoderm formation, left-right patterning and craniofacial development. *Nature*. 1998;393(6687):786–790.
19. Divakaran V, et al. Adaptive and maladptive effects of SMAD3 signaling in the adult heart after hemodynamic pressure overloading. *Circ Heart Fail*. 2009;2(6):633–642.
20. Dobaczewski M, et al. Smad3 signaling critically regulates fibroblast phenotype and function in healing myocardial infarction. *Circ Res*. 2010;107(3):418–428.
21. Hu B, Wu Z, Liu T, Ullenbruch MR, Jin H, Phan SH. Gut-enriched Krüppel-like factor interaction with Smad3 inhibits myofibroblast differentiation. *Am J Respir Cell Mol Biol*. 2007;36(1):78–84.
22. Ramirez AM, Shen Z, Ritzenthaler JD, Roman J. Myofibroblast transdifferentiation in obliterative bronchiolitis: tgf-beta signaling through smad3-dependent and -independent pathways. *Am J Transplant*. 2006;6(9):2080–2088.
23. Sato M, Muragaki Y, Saika S, Roberts AB, Ooshima A. Targeted disruption of TGF-beta1/Smad3 signaling protects against renal tubulointerstitial fibrosis induced by unilateral ureteral obstruction. *J Clin Invest*. 2003;112(10):1486–1494.
24. Saika S, et al. Smad3 signaling is required for epithelial-mesenchymal transition of lens epithelium after injury. *Am J Pathol*. 2004;164(2):651–663.
25. Wang W, et al. Essential role of Smad3 in angiotensin II-induced vascular fibrosis. *Circ Res*. 2006;98(8):1032–1039.
26. Bujak M, et al. Essential role of Smad3 in infarct healing and in the pathogenesis of cardiac remodeling. *Circulation*. 2007;116(19):2127–2138.
27. Koitabashi N, et al. Pivotal role of cardiomyocyte TGF-β signaling in the murine pathological response to sustained pressure overload. *J Clin Invest*. 2011;121(6):2301–2312.
28. Teekakirikul P, et al. Cardiac fibrosis in mice with hypertrophic cardiomyopathy is mediated by non-myocyte proliferation and requires Tgf-β. *J Clin Invest*. 2010;120(10):3520–3529.
29. Kanisicak O, et al. Genetic lineage tracing defines myofibroblast origin and function in the injured heart. *Nat Commun*. 2016;7:12260.
30. Kaur H, et al. Targeted ablation of periostin-expressing activated fibroblasts prevents adverse cardiac remodeling in mice. *Circ Res*. 2016;118(12):1906–1917.
31. Oka T, et al. Genetic manipulation of periostin expression reveals a role in cardiac hypertrophy and ventricular remodeling. *Circ Res*. 2007;101(3):313–321.
32. Snider P, Standley KN, Wang J, Azhar M, Doetschman T, Conway SJ. Origin of cardiac fibroblasts and the role of periostin. *Circ Res*. 2009;105(10):934–947.
33. Bagchi RA, Czubryt MP. Synergistic roles of scleraxis and Smads in the regulation of collagen 1α2 gene expression. *Biochim Biophys Acta*. 2012;1823(10):1936–1944.
34. Bai G, Hock TD, Logsdon N, Zhou Y, Thannickal VJ. A far-upstream AP-1/Smad binding box regulates human NOX4 promoter activation by transforming growth factor-β. *Gene*. 2014;540(1):62–67.
35. Chen S, Kulik M, Lechleider RJ. Smad proteins regulate transcriptional induction of the SM22alpha gene by TGF-beta. *Nucleic Acids Res*. 2003;31(4):1302–1310.
36. Jinnin M, Ihn H, Asano Y, Yamane K, Trojanowska M, Tamaki K. Tenascin-C upregulation by transforming growth factor-beta in human dermal fibroblasts involves Smad3, Sp1, and Ets1. *Oncogene*. 2004;23(9):1656–1667.
37. Verrecchia F, Chu ML, Mauviel A. Identification of novel TGF-beta /Smad gene targets in dermal fibroblasts using a combined cDNA microarray/promoter transactivation approach. *J Biol Chem*. 2001;276(20):17058–17062.
38. Qiu P, Feng XH, Li L. Interaction of Smad3 and SRF-associated complex mediates TGF-beta1 signals to regulate SM22 transcription during myofibroblast differentiation. *J Mol Cell Cardiol*. 2003;35(12):1407–1420.
39. Acharya A, Baek ST, Banfi S, Eskiocak B, Tallquist MD. Efficient inducible Cre-mediated recombination in Tcf21 cell lineages in the heart and kidney. *Genesis*. 2011;49(11):870–877.
40. Sohal DS, et al. Temporally regulated and tissue-specific gene manipulations in the adult and embryonic heart using a tamoxifen-inducible Cre protein. *Circ Res*. 2001;89(1):20–25.
41. Anversa P, Capasso JM, Ricci R, Sonnenblick EH, Olivetti G. Morphometric analysis of coronary capillaries during physiologic myocardial growth and induced cardiac hypertrophy: a review. *Int J Microcirc Clin Exp*. 1989;8(4):353–363.
42. Oka T, Akazawa H, Naito AT, Komuro I. Angiogenesis and cardiac hypertrophy: maintenance of cardiac function and causative roles in heart failure. *Circ Res*. 2014;114(3):565–571.
43. Accornero F, et al. Genetic analysis of connective tissue growth factor as an effector of transforming growth factor β signaling and cardiac remodeling. *Mol Cell Biol*. 2015;35(12):2154–2164.
44. Christman KL, et al. Pleiotrophin induces formation of functional neovasculature in vivo. *Biochem Biophys Res Commun*. 2005;332(4):1146–1152.
45. Christman KL, Fang Q, Yee MS, Johnson KR, Sievers RE, Lee RJ. Enhanced neovasculature formation in ischemic myocardium following delivery of pleiotrophin plasmid in a biopolymer. *Biomaterials*. 2005;26(10):1139–1144.
46. Yu W, et al. GATA4 regulates Fgf16 to promote heart repair after injury. *Development*. 2016;143(6):936–949.
47. Bujak M, Frangogiannis NG. The role of TGF-beta signaling in myocardial infarction and cardiac remodeling. *Cardiovasc Res*. 2007;74(2):184–195.
48. Meng XM, Nikolic-Paterson DJ, Lan HY. TGF-β: the master regulator of fibrosis. *Nat Rev Nephrol*. 2016;12(6):325–338.
49. Kuwahara F, et al. Transforming growth factor-beta function blocking prevents myocardial fibrosis and diastolic dysfunction in pressure-overloaded rats. *Circulation*. 2002;106(1):130–135.
50. de Kroon LM, et al. SMAD3 and SMAD4 have a more dominant role than SMAD2 in TGFβ-induced chondrogenic differentiation of bone marrow-derived mesenchymal stem cells. *Sci Rep*. 2017;7:43164.
51. Gong K, et al. Smad3-mSin3A-HDAC1 complex is required for TGF-β1-induced transcriptional inhibition of PPARγ in mouse cardiac fibroblasts. *Cell Physiol Biochem*. 2016;40(5):908–920.
52. Zhang L, Liu C, Meng XM, Huang C, Xu F, Li J. Smad2 protects against TGF-β1/Smad3-mediated collagen synthesis in human hepatic stellate cells during hepatic fibrosis. *Mol Cell Biochem*. 2015;400(1-2):17–28.
53. Yu J, et al. Identification of the gene transcription and apoptosis mediated by TGF-beta-Smad2/3-Smad4 signaling. *J Cell Physiol*. 2008;215(2):422–433.
54. Molkentin JD, et al. Fibroblast-Specific Genetic Manipulation of p38 Mitogen-Activated Protein Kinase In Vivo Reveals Its Central Regulatory Role in Fibrosis. *Circulation*. 2017;136(6):549–561.
55. Rosenbloom J, Ren S, Macarak E. New frontiers in fibrotic disease therapies: The focus of the

Joan and Joel Rosenbloom Center for Fibrotic Diseases at Thomas Jefferson University. *Matrix Biol*. 2016;51:14–25.
56. Accornero F, Kanisicak O, Tjondrokoesoemo A, Attia AC, McNally EM, Molkentin JD. Myofiber-specific inhibition of TGFβ signaling protects skeletal muscle from injury and dystrophic disease in mice. *Hum Mol Genet*. 2014;23(25):6903–6915.
57. Yamamoto M, et al. A multifunctional reporter mouse line for Cre- and FLP-dependent lineage analysis. *Genesis*. 2009;47(2):107–114.
58. Park BV, et al. TGFβ1-mediated SMAD3 enhances PD-1 expression on antigen-specific T cells in cancer. *Cancer Discov*. 2016;6(12):1366–1381.
59. Liu R, et al. Cardiac-specific deletion of protein phosphatase 1β promotes increased myofilament protein phosphorylation and contractile alterations. *J Mol Cell Cardiol*. 2015;87:204–213.
60. Nagueh SF, et al. Recommendations for the evaluation of left ventricular diastolic function by echocardiography: an update from the American Society of Echocardiography and the European Association of Cardiovascular Imaging. *Eur Heart J Cardiovasc Imaging*. 2016;17(12):1321–1360.
61. Khalil H, et al. Caspase-3 protects stressed organs against cell death. *Mol Cell Biol*. 2012;32(22):4523–4533.
62. Karch J, Kanisicak O, Brody MJ, Sargent MA, Michael DM, Molkentin JD. Necroptosis interfaces with MOMP and the MPTP in mediating cell death. *PLoS One*. 2015;10(6):e0130520.